Coherently coupling distinct spin ensembles through a high-Tc superconducting resonator

Multiple coupling of distinct spin ensembles with a high T_c superconducting resonator

A. Ghirri,[1*] C. Bonizzoni,[1,2] F. Troiani,[1†] N. Buccheri,[3] L. Beverina,[3] A. Cassinese,[4] M. Affronte[1,2]
[1] *Istituto Nanoscienze - CNR, via Campi 213/a, 411125 Modena, Italy;*
[2] *Dipartimento FIM, Università di Modena e Reggio Emilia, via Campi 213/a, 411125 Modena, Italy;*
[3] *Università di Milano-Bicocca, Dipartimento di Scienza dei Materiali, Via R. Cozzi 53, 20125 Milano, Italy.*
[4] *CNR-SPIN and Dipartimento di Fisica, Università di Napoli Federico II, 80138 Napoli, Italy;*

(Dated: April 28, 2016)

The problem of coupling distinct ensembles of two level systems through photons in a quantum box is revisited by using organic radicals (spin 1/2) and a high T_c superconducting coplanar resonator with which an exceptionally strong coupling is obtained. Up to three spin ensembles are simultaneously coupled and are made physically distinguishable by chemically varying the g factors and by exploiting the inhomogeneities of the applied magnetic field. The observed multiple anticrossing, along with the simulations performed within the input-output formalism, demonstrate the coherent coupling.

PACS numbers: 33.90.+h, 75.50.Xx, 76.30Rn, 03.67.-a, 07.57.Pt

Controlling light-matter interaction at the quantum level is a central problem in modern physics and technology. The paradigmatic system for such investigation is represented by a two-level quantum emitter coupled to a spatially confined mode of the electromagnetic field [1]. Here, the experimental benchmark of a coherent light-matter interaction is the creation of hybridized light-matter modes, which can be observed if the coupling between the field and the emitter is larger than the ones between system and environment. This strong-coupling regime has been achieved by employing a variety of quantum emitters, ranging from Rydberg atoms to superconducting qubits, all characterized by large electric-dipole transition amplitudes [2]. Spin-photon interaction is much weaker, but can be significantly enhanced by exploiting cooperative phenomena in N-spin ensembles, leading to a $\sqrt{N}$ enhancement of the spin-photon coupling constant [3, 4]. In this way, the strong coupling regime has been demonstrated with different spin systems in high quality factor microwave resonators [5–8]. Along the same lines, experimental evidence of the coherent coupling of 3D-cavity photons and magnons in ferro- and ferri-magnetic crystals has been provided [9–11].

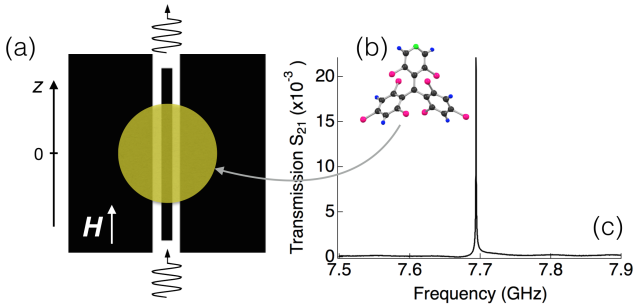

FIG. 1: (a) Measured transmission spectral map ($T = 2$ K) with a PyBTM ensemble positioned at the center. The left inset shows the molecular structure of the PyBTM molecule (Colors: C, black; Cl, magenta; N, green; H, blue). The right inset shows the representation of the YBCO coplanar resonator loaded with the PyBTM ensemble. (b) Temperature dependence of the collective coupling rate $g_1/2\pi$ of different PyBTM ensembles (symbols). Solid lines show the measured temperature dependence of the polarization factor $p(T)$, for the same spin ensembles. The temperature dependences of the spin (γ_1) and cavity (κ) decay rates are shown for comparison.

In the last years, molecular spin systems have revealed interesting potentialities for quantum-information processing [12], such as a wide tunability of the physical parameters and decoherence times exceeding 10^3 the gating times at liquid nitrogen temperature [13–16]. Organic radicals provide possibly the simplest spin systems, consisting of single unpaired electrons with isotropic g-factors. In addition, the presence of intermolecular exchange interactions in non-diluted ensembles gives rise to the exchange narrowing effect, which averages out the intermolecular dipolar and hyperfine interactions and typically give rise to magnetic dipolar transitions with Lorentzian line shape and reduced line width [17]. Spin ensembles of organic radicals can thus combine narrow magnetic transitions and high spin densities. For this reason, they are particularly suitable for reaching the strong coupling regime in a microwave cavity [18–20], while their versatility inspires the implementation of quantum gates [21].

Here we exploit these features of molecular spin systems in order to demonstrate the coherent coupling between distinguishable spin ensembles. By using (3,5-dichloro-4-pyridyl)bis(2,4,6-trichlorophenyl)methyl radi-

*alberto.ghirri@nano.cnr.it
†Corresponding author. filippo.troiani@unimore.it

cals (PyBTM) [22], we first show that the strong-coupling regime is largely fulfilled in a broad temperature range, with values of the cooperativity reaching 4300 at 2 K. Due to this large cooperativity, we can provide an experimental evidence of the coherent coupling between up to three remote spin ensembles mediated by the cavity mode of a high T_c YBCO/sapphire coplanar resonator. This can represent a resource for the implementation of hybrid architectures and of quantum-information approaches based on the use of multiple spin-excitation modes.

Our experiment consists in measuring the transmission spectrum of a coplanar resonator in the presence of one or more ensembles of spin radicals. An external magnetic field, applied in the plane of the superconducting film along the z axis (Fig. 1), is used to tune the Zeeman energy of the spins, and thus their detuning with respect to the energy of the cavity mode. The YBCO resonators allow us to expand the ranges of temperature, magnetic field and power, with respect to the Nb cavities, which are commonly used in circuit-QED experiments. Notably, the resonance frequency and the quality factor of the bare YBCO resonator are, at low temperature, weakly dependent on the external magnetic field [20]. The resonator is installed in a cryo-magnetic set-up [23] and the transmission scattering parameter (S_{21}) is measured by means of a vector network analyzer. When the sample is positioned at the center of the resonator, in zero field the fundamental mode has a frequency $\omega_c/2\pi \simeq 7.7\,\mathrm{GHz}$ and a quality factor $Q \simeq 2.3 \times 10^4$, which correspond to a cavity decay rate $\kappa/2\pi = \omega_c/2\pi Q \simeq 0.3\,\mathrm{MHz}$. Typical incident power in our experiments is -13 dBm, corresponding to an average number of photons in the cavity of approximately $10^{12} - 10^{14}$.

To grasp the essential Physics, we consider a system formed by M ensembles of $s = 1/2$ spins, coupled to a single mode of the cavity. Within the rotating-wave approximation, this is described by the Tavis-Cummings Hamiltonian ($\hbar \equiv 1$) [4]:

$$H_{TC} = \omega_c a^\dagger a + \sum_{k=1}^{M} [\omega_k S_{z,k} + \eta_k (a^\dagger S_{k,-} + a S_{k,+})], \quad (1)$$

where ω_c is the frequency of the cavity mode, ω_k the Zeeman splitting of a spin belonging to the k-th spin ensemble, and η_k the coupling between each of such spins and the cavity mode. In the low-excitation limit (*i.e.* if the number of excitations is much smaller than the number of spins N_k in each spin ensemble), one can introduce the Holstein-Primakoff transformation [24], where the states of each spin ensemble are mapped onto those of a bosonic mode. As a result, the system Hamiltonian becomes:

$$H = w_c a^\dagger a + \sum_{k=1}^{M} [\omega_k (b_k^\dagger b_k - S_k) + g_k (a^\dagger b_k + b_k^\dagger a)], \quad (2)$$

where $g_k = \eta_k \sqrt{2S_k}$ is the collective coupling between the spin ensemble and the cavity mode [23]. In order to simulate the observed spectra, we make use of the standard input-output formalism [25]. The relations between the input and output modes of the two-sided cavity can be obtained by combining the two equations that define the boundary conditions for the cavity with the $M + 1$ Heisenberg equations for the field and spin-ensemble annihilation operators. The elements of the scattering matrix are given by

$$S_{21} = \frac{\sqrt{\kappa_1 \kappa_2}}{i(\omega_c - \omega) + \frac{1}{2}(\kappa_1 + \kappa_2 + \kappa_{int}) + \sum_{k=1}^{M} \frac{g_k^2}{i(\omega_k - \omega) + \gamma_k/2}}, \quad (3)$$

where κ_1 and κ_2 represent the cavity photon escape rates to the two sides of the cavity, while κ_{int} accounts for additional cavity-relaxation channels. The relaxation rate of the k-th spin mode is γ_k.

We initially considered the simplest case, where a single spin ensemble is positioned at the antinode of the magnetic field, corresponding to the center of the coplanar resonator (Fig. 1). The spin ensemble is formed by PyBTM radicals, characterized by a g-factor of 2.003. The transmission spectrum, measured as a function of the external magnetic field, displays a well-defined anticrossing [Fig. 1(a)]. The splitting between the two lines at the resonance field $B_r \simeq 0.274\,\mathrm{T}$ is about 191 MHz. The low-temperature transmission spectrum can be simulated by means of the input-output relation (Eq. 3, with $M = 1$), which is used to estimate the physical parameters of the Hamiltonian H and the relevant relaxation rates. The best fit between the measured and the computed spectra is obtained for $g_1 = 95\,\mathrm{MHz}$ and $\gamma_1 = 7\,\mathrm{MHz}$ [23]. The estimated rates of the cavity-photon loss to the input and output modes are $\kappa_1 = \kappa_2 \simeq 4\,\mathrm{kHz}$. The cavity-photon lifetime is however limited by the internal

Fig2.png

FIG. 2: Transmission spectroscopy experiments with two spin ensembles. Schematics of the superconducting resonator loaded with: (a) two PyBTM samples at the center; (d) one PyBTM and one DPPH sample at the center; (g) two PyBTM samples at the boundaries of the central electrode. In the panels (b,e,h) we show the transmission spectral map measured at 2 K; the panels (c,f,i) contain the comparison between experimental and simulated spectra at the multiple anticrossing field.

losses, being $\kappa_{int} \simeq 0.3\,\mathrm{MHz}$, as estimated by fitting the transmission spectrum far off resonance [23]. Altogether, these parameters allow us to reproduce the Lorentzian line shapes of the peaks at resonance. Being the spin-photon coupling g_1 larger than all the dissipative rates, the strong-coupling between the spin ensemble and the cavity mode is clearly achieved, with values of the cooperativity $C = g_1^2/\gamma_1\kappa_1$ as high as 4300 at 2 K. Notice that this number is two order of magnitude larger than those typically reached with spin impurities in crystals [2] and even larger than those obtained with ferrimagnetic YIG coupled to coplanar resonator [9].

The transmission spectra are expected to display a temperature dependence, which can be investigated thanks to the stability of the YBCO resonator in a wide temperature range [20]. In particular, we focus on the temperature dependence of the spin-photon coupling, resulting from the thermal occupation of spin states corresponding to nonmaximal values of the total spin. The results are displayed in Fig. 1(b) for three different ensembles of PyBTM radicals and compared with the square root of the polarization factor $p(T) = 2\overline{M}/N \leq 1$ (solid lines), which are independently derived from the measurement of the average value of the magnetization ($\overline{M}$) [23]. The trends of the two quantities are indeed similar: $\overline{g^2}(T)/g^2(0) \simeq p(T)$. On the other hand, we note that the dependence of the polarization factor significantly deviates from what expected for an ensemble of uncoupled spins. This suggests that some interaction among the spins of the ensemble is indeed present. The temperature dependence of the magnetic susceptibility [23] confirms this, and additionally shows that such interactions tend to favor states with lower values of the total spin, with respect to the case of noninteracting spins. Based on the estimated value of the single-spin coupling $\eta = 0.6\,\mathrm{Hz}$ [20], we can also estimate the number of spins that form the three spin ensembles, which is of the order of 10^{17} in all three cases. Finally, the spin decay rate γ_1 monotonically increases with temperature in the range $2 - 30\,\mathrm{K}$, while the overall photon-decay rate remains below 0.5 MHz. The strong-coupling regime is thus preserved (at least) up to $T = 30\,\mathrm{K}$.

The phenomenology becomes richer when physically distinguishable spin ensembles are simultaneously coupled to the same cavity mode. Such distinguishability results from different values of the Zeeman energies, this in turn can result either from the use of spins with different values of the g-factor, or from possible inhomogeneities in the applied magnetic field. In the following, we provide examples of both approaches.

As a preliminary study, we consider the case where the previous ensembles of PyBTM radicals is divided into two parts, and these are positioned at the center of the resonator, separated by about $200\,\mu\mathrm{m}$ [Fig. 2(a)]. The transmission spectrum shows a single anticrossing as a function of the magnetic field, centered at the resonance field of PyBTM [Fig. 2(b)]. This behavior confirms that, if the two ensembles are degenerate ($\omega_1 = \omega_2$), one obtains a dark and a bright mode, the latter being characterized by an enhanced spin-photon coupling [27, 28]. The observed spectrum thus coincides with that of a single, large spin ensemble. In this case, the transmission spectrum is well reproduced by the input-output relations, with $M = 1$, $g_1^2 \simeq 95\,\mathrm{MHz}$, and $\gamma_1 = 7\,\mathrm{MHz}$, as for the spin ensemble prior to the separation.

In order to observe additional features in the transmission spectrum, we replace one of the two PyBTM ensembles with a slightly inequivalent one, formed by DPPH radicals, without modifying the system geometry. The g-factor of DPPH is 2.0037, slightly different from that of PyBTM. An additional, faint line now appears between the two main ones at the avoided level crossing, and the on-resonance transmission spectrum shows three peaks [Fig. 2(f)]. The two spin ensembles are no longer degenerate, and this induces a mixing between the bright and dark modes discussed above. Being this effect absent in the previous case, the removal of the degeneracy can be attributed, at least partially, to the slight difference in terms of g-factor between the two radicals. The transmission spectrum can be reproduced by assuming $g_1 = 50\,\mathrm{MHz}$ and $\gamma_1 = 8\,\mathrm{MHz}$ for PyBTM, $g_2 = 37\,\mathrm{MHz}$ and $\gamma_2 = 14\,\mathrm{MHz}$ for DPPH [23].

An inequivalence between two spin ensembles can also result from gradients in the applied magnetic field across the resonator. From the study of the resonance field of a DPPH reference sample as a function of its z position on the resonator, we have indeed assessed the presence of a field gradient of approximately $0.9\,\mathrm{T/m}$ directed along the z axis [23]. In order to exploit this effect, we position two identical ensembles of PyBTM at the opposite sides of the resonator, close to the boundaries of the central superconducting electrode [Fig. 2(g)]. The measured transmission spectral map [Fig. 2(h)] qualitatively reproduces the features shown in the previous case. In this case, however, being the spins that form the two ensembles physically identical, the removal of the degeneracy between the respective Zeeman energies can only be ascribed to a magnetic-field gradient. As expected, the coupling to the resonator mode is weaker than the one observed in the previously considered geometry, where all the spins are positioned at the antinode of the magnetic field. The values of the parameters that result from the fitting procedure are: $g_1 = 22\,\mathrm{MHz}$ and $g_2 = 29\,\mathrm{MHz}$, and lead to a good agreement between theory and experiment [23]. Besides, the observed line widths are significantly larger than in the previous cases, and result in the following estimate of the spin relaxation rates: $\gamma_1 = \gamma_2 = 13\,\mathrm{MHz}$. This is probably due to the inhomogeneity of static field in correspondence to the boundaries of the lithographed electrode.

The possibility to reach the strong coupling even when the spin ensembles are located at the boundaries of the central electrode allows us to study the coupling of three inequivalent spin ensembles with the resonator mode. In order to observe the peculiar features of a three-spin ensemble system, the difference between the Zeeman energies of any two ensembles must be comparable to the collective spin-photon coupling [23]. Such condition can be met on one hand by reducing the size of the PyBTM ensembles, and thus the spin-photon coupling, with respect to the ones considered so far, and, on the other hand, by tuning the difference in Zeeman energies through a

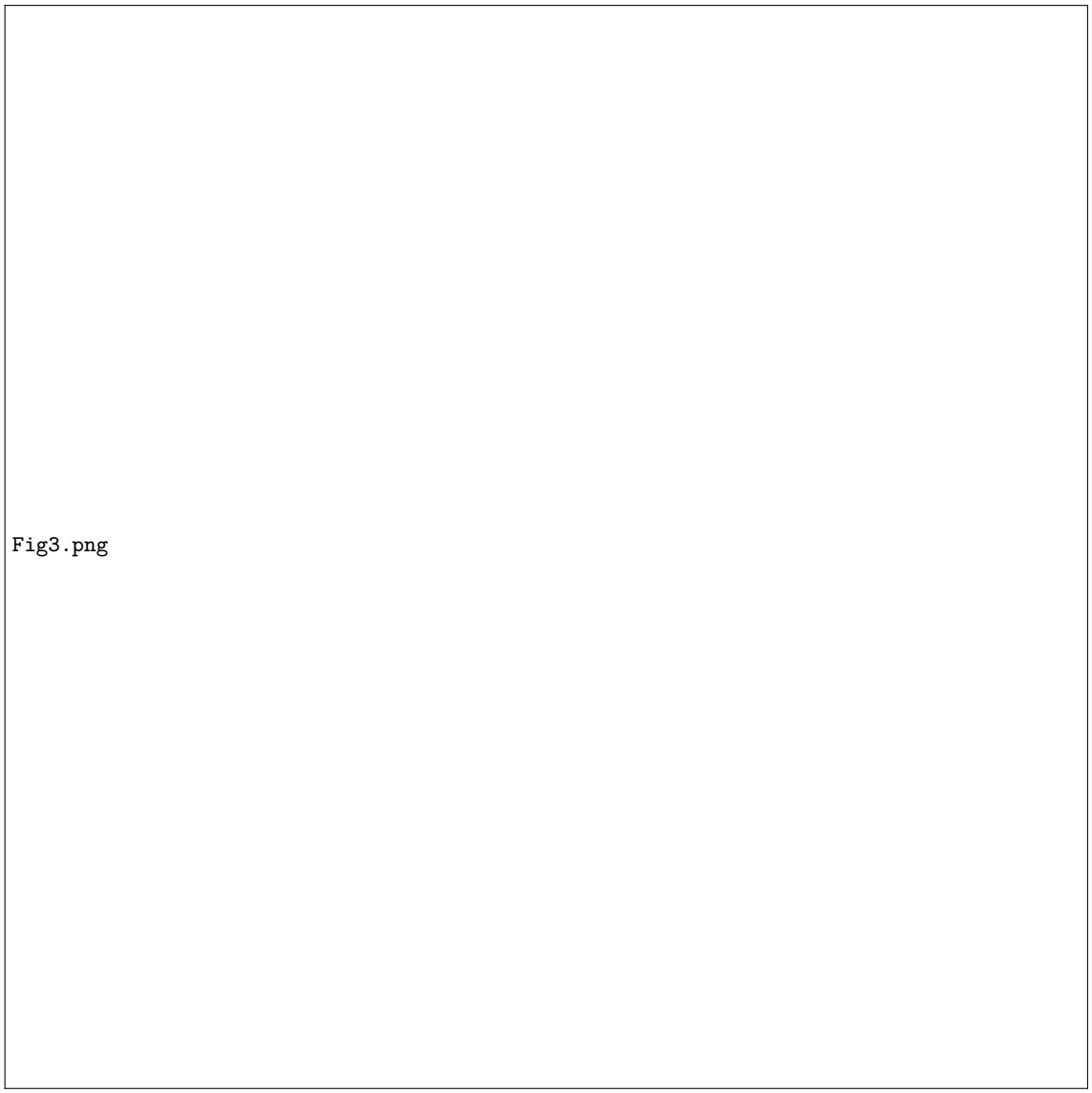

FIG. 3: Transmission spectroscopy experiments with three spin ensembles. One ensemble is positioned at the center of the resonator, while the two external ensembles are placed on the edge of the central electrode (upper row) or on the gap between the central strip and the external box (lower row). In each row we display the experimental results obtained for a given geometry (a,b) and the corresponding simulations performed through the input-output formalism (b,e). The dashed lines show the calculated eigenvalues of the system Hamiltonian. Panels (c,f) show the entropic measures $\mathcal{S}_k$, and their sum $\mathcal{S}$ calculated for the hybrid spin-photon modes, as a function of the magnetic field.

suitable positioning of the spin ensembles within the superconducting electrode. In particular, if we position one spin ensemble at the center of the resonator, and two ensembles at the edges of the central electrode, the values of the spin-photon couplings and of the detunings ($g_1 = 13\,\mathrm{MHz}$, $g_2 = 20\,\mathrm{MHz}$ and $g_3 = 49\,\mathrm{MHz}$) give rise to a multiple level crossing [Fig. 3(a,b)]. Here the cavity mode and the three spin modes are all hybridized in the same range of magnetic field values. If the two lateral spin ensembles are positioned on the gaps between the central electrode and the the external box, then the detuning between the spin ensembles, relative to the spin-photon couplings, is increased with respect to the previous case ($g_1 = 12\,\mathrm{MHz}$, $g_2 = 18\,\mathrm{MHz}$ and $g_3 = 38\,\mathrm{MHz}$). As a result, the three spin ensembles give rise to three nearly independent anticrossings, and their excitations hybridize with those of the cavity in different regions of the spectrum [Fig. 3(d,e)].

The transmission spectra obtained for two different geometries seem to present a qualitative difference. In the former case, the four hybrid spin-photon modes are all involved in a multiple anticrossing, and four lines are observable in the same range of values of the magnetic field. In the latter case, the normal modes give rise to two sequential anticrossings, each involving three lines at a time. This characterization of the anticrossings can be put on a quantitative basis by introducing an entropic

measure of the coherent mode mixing, such as

$$S = \sum_{k=1}^{M+1} S_k = \sum_{k,l=1}^{M+1} (\mu_l^k)^2 \log_2(\mu_l^k)^2. \quad (4)$$

Here, the entropy S_k tells us to which extent the normal mode c_k is distributed amongst the resonator mode a and the spin modes b_k, while S gives the overall degree of mixing that characterizes the normal modes. In the case of the first geometry in Fig. 3, all the entropies $\mathcal{S}_k$ present a maximum at approximately the same value of the field [solid colored curves in Fig. 3(c)], where the overall entropy $\mathcal{S}$ reaches its own maximum. In the case of the second geometry, the entropies S_k present two well separated maxima, one for each pair of normal modes [Fig. 3(f)]. At each of the two maxima, one of the modes has a vanishing small entropy and approximately corresponds to a non-hybridized spin mode.

In conclusion, we have demonstrated the coherent coupling between physically distinguishable ensembles of organic radicals. The fingerprint of such coupling is represented by the multiple anticrossing between hybridized spin-photon modes, observed as a function of the applied field. This observation is allowed by the slight physical difference between the spin ensembles (specifically in terms of the g-factors) and by the inhomogeneities of the applied magnetic field throughout the resonator, combined with the high cooperativity ($C \simeq 4300$) that is achieved in the device. A wider control on the generation of such coherent coupling between distinguishable and remote spin ensembles can result from the generation of strong field gradients across the resonator. In this respect, the resilience the magnetic field of the YBCO resonators offers novel opportunities. Additional possibilities arise from the wide range of g-factors that can be obtained in molecular spin systems, that open new possibilities for the realization of hybrid quantum architectures with engineered spin transitions.

The authors acknowledge M. D'Arienzo and M. Sassi for their help in the preparation and characterization of the organic sample. This work was funded by the Italian Ministry of Education and Research (MIUR) through "Fondo Investimenti per la Ricerca di Base" (FIRB) project RBFR12RPD1 and Progetto Premiale EOS, by the US AFOSR/AOARD program, contract FA2386-13-1-4029 and by the European FP7 FET project *MoQuaS* contract N.610449.

[1] E. T. Jaynes and F. W. Cummings, Proc. IEEE **51**, 89 (1963).
[2] Z.-L. Xiang, S. Ashhab, J. Q. You, and F. Nori, Rev. Mod. Phys. **85**, 623 (2013).
[3] R. H. Dicke, Phys. Rev. **93**, 99 (1954).
[4] M. Tavis and F. W. Cummings, Phys. Rev. **170**, 379 (1968).
[5] Y. Kubo, F. R. Ong, P. Bertet, D. Vion, V. Jacques, D. Zheng, A. Dréau, J. F. Roch, A. Auffèves, F. Jelezko, J. Wrachtrup, M. F. Barthe, P. Bergonzo, and D. Esteve, Phys. Rev. Lett. **105**, 140502 (2010).
[6] R. Amsüss, C. Koller, T. Nöbauer, S. Putz, S. Rotter, K. Sandner, S. Schneider, M. Schramböck, G. Steinhauser, H. Ritsch, J. Schmiedmayer, and J. Majer, Phys. Rev. Lett. **107**, 060502 (2011).
[7] D. I. Schuster, A. P. Sears, E. Ginossar, L. DiCarlo, L. Frunzio, J. J. L. Morton, H. Wu, G. A. D. Briggs, B. B. Buckley, D. D. Awschalom, and R. J. Schoelkopf, Phys. Rev. Lett. **105**, 140501 (2010).
[8] S. Probst, H. Rotzinger, S. Wünsch, P. Jung, M. Jerger, M. Siegel, A.V. Ustinov, and P. A. Bushev, Phys. Rev. Lett. **110**, 157001 (2013).
[9] H. Huebl, C. W. Zollitsch, J. Lotze, F. Hocke, M. Greifenstein, A. Marx, R. Gross and S. T. B. Goennenwein, Phys. Rev. Lett. **111**, 127003 (2013).
[10] Y. Tabuchi, S. Ishino, T. Ishikawa, R. Yamazaki, K. Usami, and Y. Nakamura, Phys. Rev. Lett. **113**, 083603 (2014).
[11] X. Zhang, C.-L. Zou, L. Jiang, and H. X. Tang, Phys. Rev. Lett. **113**, 156401 (2014).
[12] A. Ghirri, F. Troiani, and M. Affronte, in *Molecular Nanomagnets and Related Phenomena - Structure and Bonding* (Edited by: S. Gao, Springer, Berlin, 2015).
[13] M. Warner, S. Din, I. S. Tupitsyn, G. W. Morley, A. M. Stoneham, J. A. Gardener, Z. Wu, A. J. Fisher, S. Heutz, C. W. M. Kay and G. Aeppli, Nature **503**, 504 (2013).
[14] K. Bader, D. Dengler, S. Lenz, B. Endeward, S.-D. Jiang, P. Neugebauer and J. van Slageren, Nat. Commun. **5**, 5304 (2014).
[15] J. M. Zadrozny, J. Niklas, O. G. Poluektov, and D. E. Freedman, ACS Cent. Sci. **1**, 488 (2015).
[16] M. Atzori, L. Tesi, E. Morra, M. Chiesa, L. Sorace and R. Sessoli, J. Am. Chem. Soc. **138**, 2154 (2016).
[17] A. Abragam and B. Bleaney, *Electron Paramagnetic Resonance of Transition Ions* (Clarendon Press, Oxford, 1970).
[18] I. Chiorescu, N. Groll, S. Bertaina, T. Mori, and S. Myiashita, Phys. Rev. B **82** 024413 (2010).
[19] E. Abe, H. Wu, A. Ardavan, and J. J. L. Morton, Appl. Phys. Lett. **98**, 251108 (2011).
[20] A. Ghirri, C. Bonizzoni, D. Gerace, S. Sanna, A. Cassinese and M. Affronte, Appl. Phys. Lett. **106**, 184101 (2015).
[21] K. Sato, S. Nakazawa, R. Rahimi, T. Ise, S. Nishida, T. Yoshino, N. Mori, K. Toyota, D. Shiomi, Y. Yakiyama, Y. Morita, M. Kitagawa, K. Nakasuji, M. Nakahara, H. Hara, P. Carl, P. Hofer and T. Takui, J. Mater. Chem. **19**, 3739 (2009).
[22] Y. Hattori, T. Kusamoto and H. Nishihara, Angew. Chem. Int. Ed. **53**, 11845 (2014).
[23] See Supplemental Material at [URL will be inserted by publisher] for experimental details, theoretical background and input-output simulations.
[24] T. Holstein and H. Primakoff, Phys. Rev. **58**, 1098 (1940).
[25] D. F. Walls and G. J. Milburn, *Quantum optics* (Springer-Verlag, Berlin, 1994).
[26] K. Sandner, H. Ritsch, R. Amsüss, Ch. Koller, T. Nöbauer, S. Putz, J. Schmiedmayer, and J. Majer, Phys. Rev. A **85**, 053806 (2012).
[27] Z. Kurucz, J. H. Wesenberg and K. Molmer, Phys. Rev. A **83**, 053852 (2011).

[28] I. Diniz, S. Portolan, R. Ferreira, J. M. Gerard, P. Bertet and A. Auffeves, Phys. Rev. A **84**, 063810 (2011).